Steel and Composite Structures, *Vol. 30, No. 2 (2019) 171-183*
DOI: https://doi.org/10.12989/scs.2019.30.2.171

Square CFST columns under cyclic load and acid rain attack: Experiments

Fang Yuan [a], Mengcheng Chen [*] and Hong Huang [b]

Department of Civil Engineering and Architecture, East China Jiaotong University, Nanchang, 330013, China

(*Received July 13, 2018, Revised December 29, 2018, Accepted January 22, 2019*)

Abstract. As China's infrastructure continues to grow, concrete filled steel tubular (CFST) structures are attracting increasing interest for use in engineering applications in earthquake prone regions owing to their high section modulus, high strength, and good seismic performance. However, in a corrosive environment, the seismic resistance of the CFST columns may be affected to a certain extent. This study attempts to investigate the mechanical behaviours of square CFST members under both a cyclic load and an acid rain attack. First, the tensile mechanical properties of steel plates with various corrosion rates were tested. Second, a total of 12 columns with different corrosion rates were subjected to a reversed cyclic load and tested. Third, comparisons between the test results and the predicted ultimate strength by using four existing codes were carried out. It was found that the corrosion leads to an evident decrease in yield strength, elastic modulus, and tensile strain capacity of steel plates, and also to a noticeable deterioration in the ultimate strength, ductility, and energy dissipation of the CFST members. A larger axial force ratio leads to a more significant resulting deterioration of the seismic behaviour of the columns. In addition, the losses of both thickness and yield strength of an outer steel tube caused by corrosion should be taken into account when predicting the ultimate strength of corroded CFST columns.

Keywords: concrete filled steel tubular (CFST) columns; acid rain attack; experiments; cyclic load; seismic performance

1. Introduction

With the rapid growth in infrastructure in China, concrete filled steel tubes (CFSTs) are being increasingly utilized owing to their strength, good ductility, and excellent energy dissipation capacity (Evirgen *et al*. 2014, Aslani *et al*. 2017, Ghazijahani *et al*. 2017, Kharoob *et al*. 2017). Industrial and urban developments have increased the amount of acid rain worldwide, particularly in China. Acid rainfall has been reported to cover at least one-third of Chinese territory (Larssen *et al*. 1999, Hill *et al*. 2003, Aslani *et al*. 2015, Patel *et al*. 2016). In addition, China is a multi-seismic country. Therefore, CFST structures in China have been suffering significantly from deterioration owing to long-term corrosion and earthquake disasters. Thus, studies on the seismic behaviours of CFST members under corrosive environments, for example, acid rain, are of significant importance.

A large number of studies have been carried out on the seismic behaviours of CFST members (Sakino and Tomii 1981, Morishita and Tomii 1982, Boyd *et al*. 1995, Hajjar *et al*. 1998, Lahlou *et al*. 1999, Nakanishi *et al*. 1999, Elremaily and Azizinamini 2002). Literature reviews have been conducted by Nakanishi *et al*. (1999) and Elremaily and Azizinamini (2002), whose results indicate that the ductility of CFST members is much higher than that of hollow steel tubes owing to the composite effect of the outer steel and core concrete. Rezaifar and Younesi (2017) tested the seismic behaviour of internal/external stiffeners in rigid beam-to-concrete filled steel tube and hollow steel section column connections. The test results showed that the plastic hinge moves away from the column face due to their specific geometry.

Studies into constructional steel and CFST structures subjected to corrosive environments have also been conducted in recent years. For example, Melchers (2006) studied the influential factors on the corrosion rate of steel in seawater environments. Saad-Eldeen *et al*. (2013) tested the ultimate strength of a corroded steel box girder. Sultana *et al*. (2015) studied the compressive strength of stiffened panels under pitted corrosion. Karagah *et al*. (2015) tested the steel columns under corrosion and axial compression. Han *et al*. (2012, 2014) and Hou *et al*. (2016) carried out experiments on large numbers of beams and stub columns under sustained load and chloride corrosion. It was found that corrosion has a significant effect on the ultimate strength of CFST members. Simplified calculation methods for the residual strength of CFST stub columns and beams were also proposed based on parametric studies (Hou *et al*. 2016).

Previous studies have focused on the static behaviours of corroded CFST members. Few experiments have been conducted on the seismic behaviours of corroded CFST members, however, particularly under acid rain attack, giving rise to the need for more studies on this type of problem.

This study aims to investigate the seismic behaviours of

*Corresponding author, Ph.D., Professor, E-mail: mcchen@ecjtu.edu.cn
[a] Ph.D., Associate Professor, E-mail: fyuan@ecjtu.edu.cn
[b] Ph.D., Professor, E-mail: huanghong1977@foxmail.com

http://www.techno-press.org/?journal=scs&subpage=6
ISSN: 1229-9367 (Print), 1598-6233 (Online)

square CFST members under acid rain attack. The influence of corrosion on the mechanical behaviours of a steel plate is first discussed. Next, the effects of the corrosion rate and axial force ratio on the seismic behaviours of CFST columns, such as the ultimate strength, ductility, and energy dissipation ability, are systematically evaluated. Finally, comparisons between the predictions of ultimate strength from the existing codes and the measured results are carried out.

2. Experimental program

2.1 Preparation of specimens

Totally 12 square CFST columns were tested in the present work. All tested specimens have a sectional size of $L \times B \times t_{s0}$ = 1500 × 114 × 3.64 mm, where L is the column length, and B and t_{s0} are the width and initial wall thickness of the steel tube, respectively. The steel tubes were manufactured by cutting plates from a mild steel sheet and welding into a square shape with butt welds. Before casting, one end of the steel tube was sealed by welding a steel plate. The concrete was then cast into the steel tube and vibrated synchronously with a poker. A small amount of shrinkage was observed at the top of the column before testing, which was filled by a high strength epoxy to make the top end of the steel tube flush with the concrete surface. Before testing, the column was sealed by welding another steel plate on to the top end of the steel tube. The main design parameters are an axial force ratio (n) varying from 0 to 0.5 and a corrosion rate (η) of 0 to 30%. The axial force ratio used herein is defined as

$$n = \frac{N_0}{N_u} \tag{1}$$

where N_0 is the axial force, and N_u is the axial load capacity, which is calculated according to the simplified formulas described in code DB36/J001 (2007). The corrosion rate is defined as

$$\eta = \frac{t_{s0} - t_s}{t_{s0}} \times 100\% \tag{2}$$

where t_s is the remaining thickness after corrosion. The corrosion rates are designed to be 0, 10%, 20%, and 30%.

Table 1 shows a summary of the tested specimen information, where ξ represents the confinement factor of CFST members, and was defined by Han *et al*. (2012) as follows

Table 1 Information of column specimens

No.	Specimen ID	B (mm)	t_s (mm)	L (mm)	f_{cu} (MPa)	n	η (%)	ξ	Yield		Ultimate	
									P_y (kN)	Δ_y (mm)	P_u (kN)	Δ_u (mm)
1	SC0.2-0	114	3.64	1500	50	0.2	0	1.61	77.84	14.05	103.15	34.53
2	SC0.2-10	114	3.25	1500	50	0.2	10.60	1.26	66.56	13.03	85.41	32.49
3	SC0.2-20	114	2.97	1500	50	0.2	18.40	1.04	58.58	11.99	74.40	22.42
4	SC0.2-30	114	2.50	1500	50	0.2	31.29	0.88	34.17	8.85	44.63	17.80
5	SC0.4-0	114	3.64	1500	50	0.4	0	1.61	73.85	10.97	99.50	32.80
6	SC0.4-10	114	3.22	1500	50	0.4	11.62	1.25	55.25	9.93	82.00	28.90
7	SC0.4-20	114	2.92	1500	50	0.4	19.65	1.02	52.60	9.01	77.08	26.84
8	SC0.4-30	114	2.49	1500	50	0.4	31.46	0.88	37.98	7.96	51.40	14.28
9	SC0.5-0	114	3.64	1500	50	0.5	0	1.61	68.00	10.05	98.50	29.29
10	SC0.5-10	114	3.27	1500	50	0.5	10.21	1.27	63.46	10.00	89.50	24.07
11	SC0.5-20	114	2.92	1500	50	0.5	19.84	1.02	44.10	9.20	67.50	19.30
12	SC0.5-30	114	2.49	1500	50	0.5	31.56	0.88	25.00	5.70	31.08	--

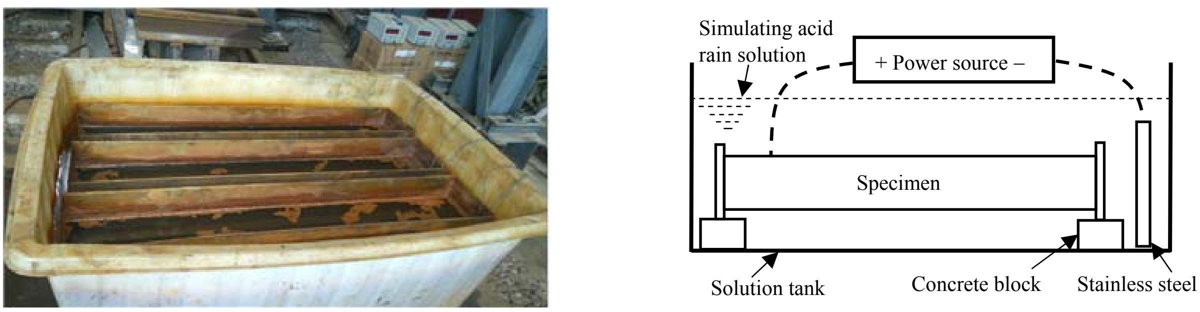

(a) Photograph of real corrosion test (b) A schematic view of corrosion test

Fig. 1 Accelerated corrosion test setup

$$\xi = \frac{A_s f_y}{A_c f_{ck}} \tag{3}$$

where A_{s0} and A_c are the initial cross-sectional areas of the steel tube and the core concrete, respectively, f_y and f_{ck} are the yield strength of steel and the characteristic compressive strength of concrete, respectively. f_{ck} is determined to be 67% of the cube strength of concrete (f_{cu}). The following naming rules of the specimens are described as follows: (1) the two initial characters, 'SC', indicate the square column sections, (2) the Arabic numbers before the hyphen are the axial force ratio, and (3) the Arabic numbers after the hyphen are the corrosion rate. For example, specimen 'SC0.2-10' indicates a square column with a designed axial force ratio of 0.2 and a corrosion rate of 10%.

2.2 Corrosion test configuration

The testing of the column specimen was divided into two stages: an accelerated corrosion test in the first stage, and an ultimate strength test in the second. The setup of the accelerated corrosion test used a water tank, stainless steel cage, an electrolytic solution, and a power source. The corrosive environment was simulated using an acid rain solution and applied direct current. The simulated acid rain solution was composed of Na_2SO_4, $(NH_4)_2SO_4$, $MgSO_4$, $Ca(NO_3)_2$, and HNO_3, based on the components of acid rain distribution in southern China (Chen *et al.* 2013). The content of Na_2SO_4, $(NH_4)_2SO_4$, $MgSO_4$, and $Ca(NO_3)_2$ solvent per liter of simulated acid rain solution was 0.99 gram, 0.13 gram, 0.24 gram and 0.16 gram, respectively. The main cations include H^+, NH^{4+}, Mg^{2+}, and Ca^{2+}, whereas the main anions include SO_4^{2-} and NO_3^-. The corrosion of constructional steel is mainly caused by H^+ and SO_4^{2-}. The pH value of the solution is determined using HNO_3, and is fixed at 2.3. The corrosion current path was achieved through connecting the outer steel tube to the anode of the power source and connecting the stainless steel to the cathode of the power source, as shown in Fig. 1. The steel plates used at the two ends of the CFST specimens were covered with fan antirust material. As a result, only the outer steel tube surfaces corroded.

In addition to the CFST specimen tests, four groups of steel coupons with corrosion rates of 0 to 30% were also tested using the accelerated corrosion method, and then tested to monitor the deterioration of the tensile properties of the steel. The test used a constant current intensity of 200 $\mu A/cm^2$ to accelerate the corrosion of the specimens. According to Faraday's law of electrochemical corrosion, the time durations to achieve the corrosion rates of 10%, 20%, and 30% are 2 months, 4 months, and 6 months, respectively. Three parallel steel coupons were prepared, corresponding to each corrosion rate. Only the surface of perpendicular to the normal direction of the steel coupons was exposed to the corrosive environment in order to simulate the practical corrosion conditions of the outer steel tubes. The corrosion rate was controlled through an adjustment of the current intensity and time of immersion. To verify the designed corrosion rate of the setup, steel coupons were first tested prior to the CFST specimen tests. The loss of thickness of the steel plate was monitored carefully during the corrosion process. The surfaces of the steel coupons and the CFST columns were cleaned after corrosion. The corrosion rate was determined by two types of approaches: weighing the tested specimens, and measuring the average thickness of the steel plate. It was found that the thickness losses measured using these two methods show a high level of consistency.

2.3 Material properties

The measured elastic modulus, yield strength, and ultimate strength of the uncorroded steel coupons are 187 GPa, 383 MPa and 516 MPa, respectively. A tensile test of the corroded steel coupons with different losses was also carried out, and detailed discussions on the mechanical properties are provided in the following sections. One type of concrete with the mixture proportions shown in Table 2

Table 2 Mixture proportions of concrete

Matrix	Cement	Water	Sand	Coarse aggregate
Concrete	1.0	0.4	1.1	2.56

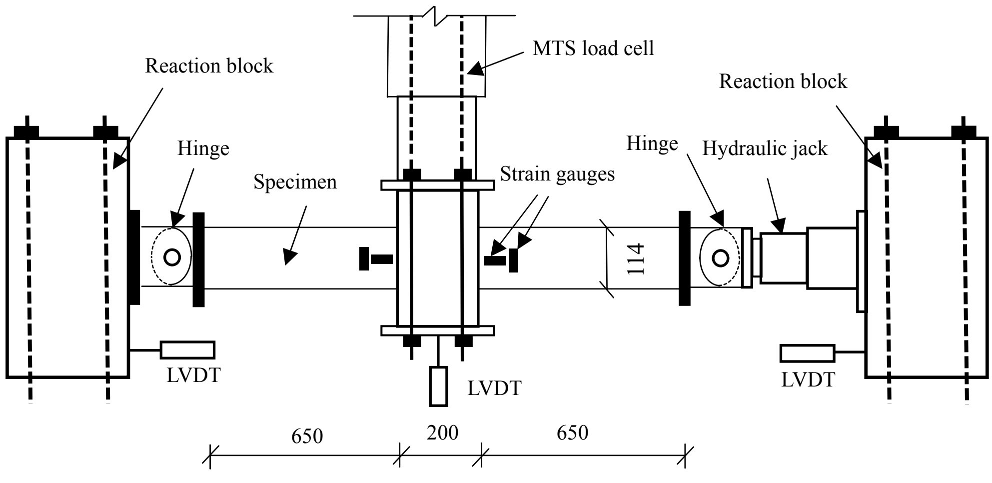

Fig. 2 Schematic cyclic loading test setup

Table 2 was designed. The measured cube strength (f_{cu}) at the time of testing is 50 MPa.

2.4 Cyclic loading configuration

The CFST columns were tested under a fixed axial force and increasing cyclic displacement. The schematic cyclic loading test setup is shown in Fig. 2. The two ends of the columns were attached to the pin supports, which were free to rotate to simulate the pin-pin end conditions. The axial load was first applied to the column through a hydraulic jack. The flexural cyclic load was then applied at the middle of the column through an MTS hydraulic ram. The cyclic load was applied at intervals of 0.25% of the estimated yield load P_y before yielding. After the yield point, the flexural cyclic load was carried out under displacement control at intervals of one yield displacement Δ_y. Three cycles were imposed at each displacement level. Fig. 3 shows the whole loading history. The test was terminated when the residual strength of the column decreased to 85% of its peak strength.

The instrumentation of the test included the measurements of lateral load and displacement, horizontal load of the hydraulic jack, horizontal displacement of the two ends of the concrete blocks, and the strains in the steel tubes near the loading point of each column. The detailed measurement arrangements are clearly shown in Fig. 2.

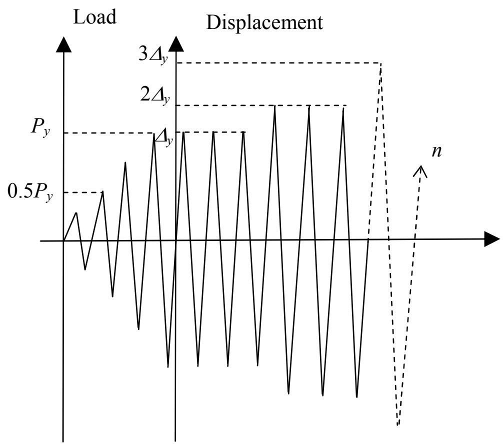

Fig. 3 Cyclic loading history

3. Results and discussions

3.1 Effects of corrosion on the mechanical properties of steel

Fig. 4 shows the effects of the corrosion rate on the mechanical properties of steel coupons, such as the elastic

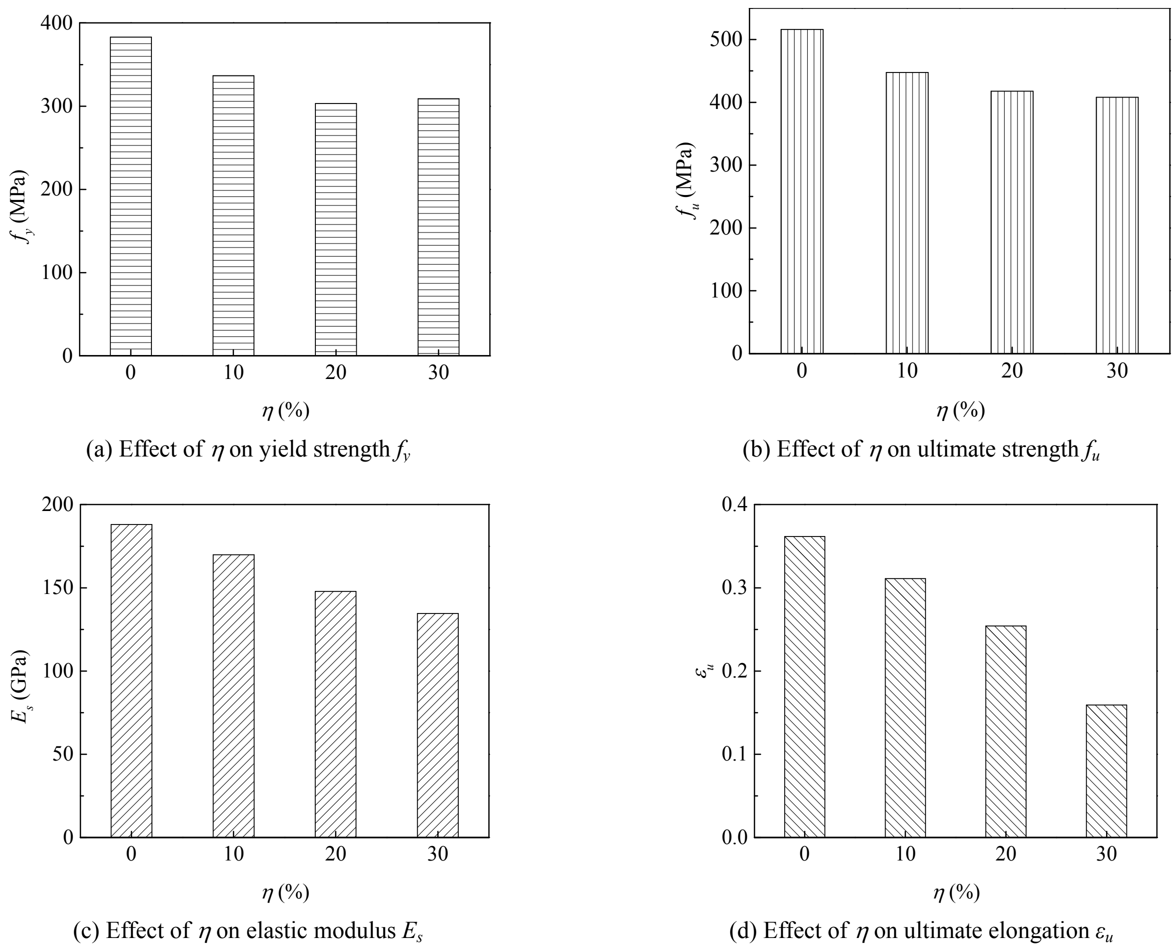

(a) Effect of η on yield strength f_y

(b) Effect of η on ultimate strength f_u

(c) Effect of η on elastic modulus E_s

(d) Effect of η on ultimate elongation ε_u

Fig. 4 Effect of corrosion rate (η) on the mechanical properties of steel

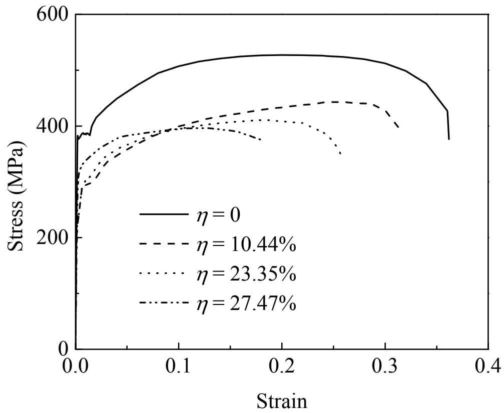

Fig. 5 Effect of corrosion rate (η) on the stress-strain response of steel

modulus (E_s), yielding strength (f_y), ultimate strength (f_u), and ultimate elongation (ε_u), which were all calculated based on actual area of corroded section. The ultimate elongation refers to the steel strain at fracture. The full-range tensile stress-strain curves of the steel coupons with different corrosion rates are also shown together in Fig. 5. It can be clearly seen that decreasing trends of E_s, f_y, f_u, and ε_u occur as the corrosion rate (η) increases. It makes sense as the large pit is more prone to occur for steel coupons with higher corrosion rate. Under the tensile load, an initial crack will appear from the largest pit and develop along the thinnest section, leading to a lower yield strength. This phenomenon is consistent with the test observations reported in most existing studies (Vu *et al*. 2009, Fernandez *et al*. 2015) but not in Almusallam (2001) which reported that the ultimate strength of rebars were not affected by corrosion. It indicates that acid rain corrosion on the steel tubes results in not only a loss in wall thickness of the steel tube but also a reduction of the tensile strength and the occurrence of deformations. Only the effective loss of thickness of a steel tube has been considered in the derivation of the simplified strength models of corroded CFST members in most existing studies (Han *et al*. 2012, 2014, Hou *et al*. 2016). As pointed out by Han *et al*. (2001), the confinement factor (ξ) plays an important role in the mechanical behaviours of CFST stub columns, columns, and beam columns. It can be inferred from Eq. (3) that both the cross-sectional area of a steel tube (A_s), which is dependent on the wall thickness (t_s), and the yield strength of the steel have positive effects on ξ. Therefore, ignorance regarding the influence of corrosion on the yield strength of a steel tube will result in non-negligible errors in the prediction of the load carrying capacity of CFST members.

The variations in the mechanical properties of steel based on the corrosion rate (η) were quantitatively analysed. The linear relationship between these factors and η was shown to regress to an approximate degree based on the experiment results of E_s, f_y, f_u, and ε_u. For more details, please refer to the test results of corroded steel coupons reported by Yuan *et al*. (2018).

3.2 Failure characteristics of CFST members

Fig. 6 shows the failure modes of the CFST columns. It can be found that a local outward buckling occurred near the loading section at midspan on the both sides of the specimen. With increasing lateral displacement, a tensile fracture occurred at the corners of the steel tube. Finally, most of the columns failed owing to tensile fracturing at the bulge location, accompanied by a rapid drop in the load resistance. The ultimate state of the other specimens without a tensile failure was reached as the lateral load decreased to 85% of its peak strength.

Fig. 6 also shows that the failure features of the corroded CFST specimens are almost the same as those of an uncorroded specimen, which indicates that corrosion does not change the failure patterns of the columns. This observation is consistent with the test observations reported by Han *et al*. (2014) and Hou *et al*. (2016).

The failure modes of the core concrete after the test are shown in Fig. 7. It can be seen that, under reversed tension and compression, an evident sign of cracking and crushing

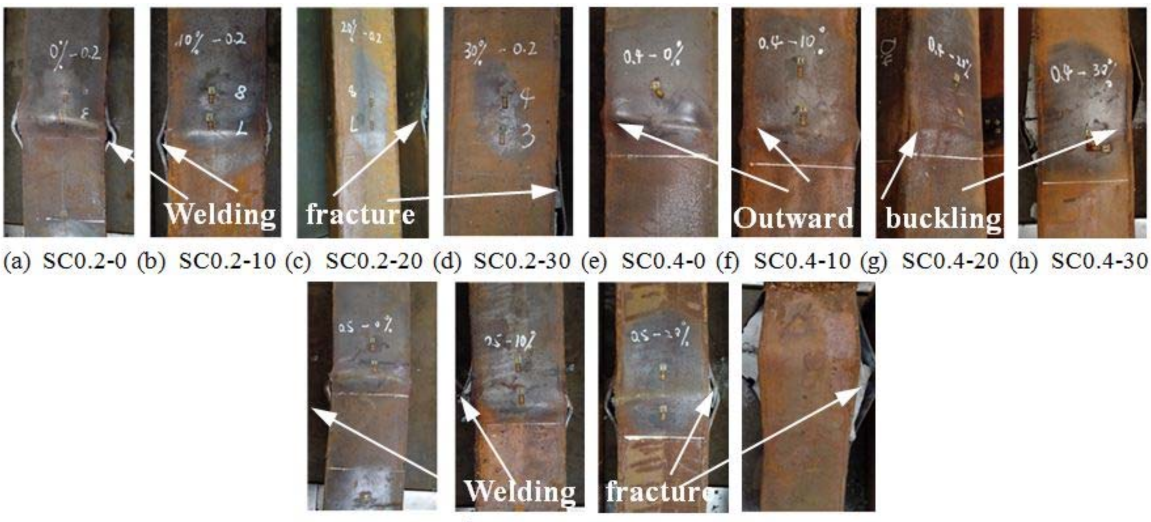

(a) SC0.2-0 (b) SC0.2-10 (c) SC0.2-20 (d) SC0.2-30 (e) SC0.4-0 (f) SC0.4-10 (g) SC0.4-20 (h) SC0.4-30

(i) SC0.5-0 (j) SC0.5-10 (k) SC0.5-20 (l) SC0.5-30

Fig. 6 Failure patterns of the specimens

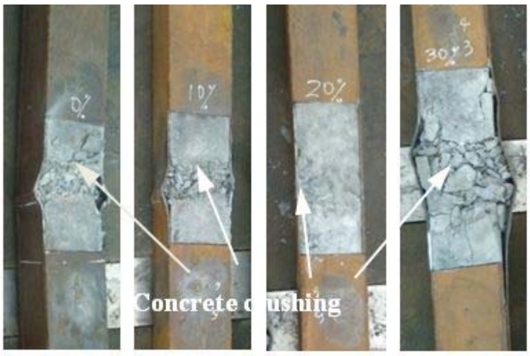

(a) SC0.2-0 (b) SC0.2-10 (c) SC0.2-20 (d) SC0.2-30

Fig. 7 Typical failure modes of core concrete in CFST

was observed within the vicinity of the loading section at midspan. Because the maximum moment occurred at the midspan section, this test observation is quite reasonable for columns under reverse lateral load.

3.3 Lateral load (P) versus lateral displacement (Δ) curves

Fig. 8 shows the lateral load versus the mid-span displacement curves (which are also called hysteresis curves) for all specimens. It is found that the hysteresis loops of the uncorroded columns are significantly plumper than those of the corroded columns. The hysteresis loop becomes increasingly smaller as the corrosion rate increases, indicating a lower capacity of energy dissipation for columns with severer corrosion. This phenomenon can be explained through the following factors. First, the steel tube thickness decreases with the increase in the corrosion rate, which results in a drop in the tensile load provided by the steel and a composite effect between the core concrete and steel tube. Second, as is well known, steel has excellent plasticity, and the outer steel tube plays an important role in the energy dissipation of CFST members. The pinching effect of the hysteresis loops will be more apparent for CFST members with a lower steel ratio. Third, as discussed above, corrosion also leads to a reduction in yield strength of a steel tube, which further reduces the confinement factor (ξ), as indicated in Eq. (3). The confinement effect will be weaker and a steel tube buckling of a steel tube will be more pronounced as ξ decreases, resulting in lower load carrying and deformation capacities, and thus smaller hysteresis loops of the CFST members.

Fig. 9 shows the load versus displacement envelop curves of the columns. The curves of the corroded specimens tend to drop more quickly than the uncorroded specimens owing to a premature buckling of the steel tubes. The load carrying capacity decreases and the area encompassed by the curve decreases as the corrosion rate increases at each axial force level. For example, the

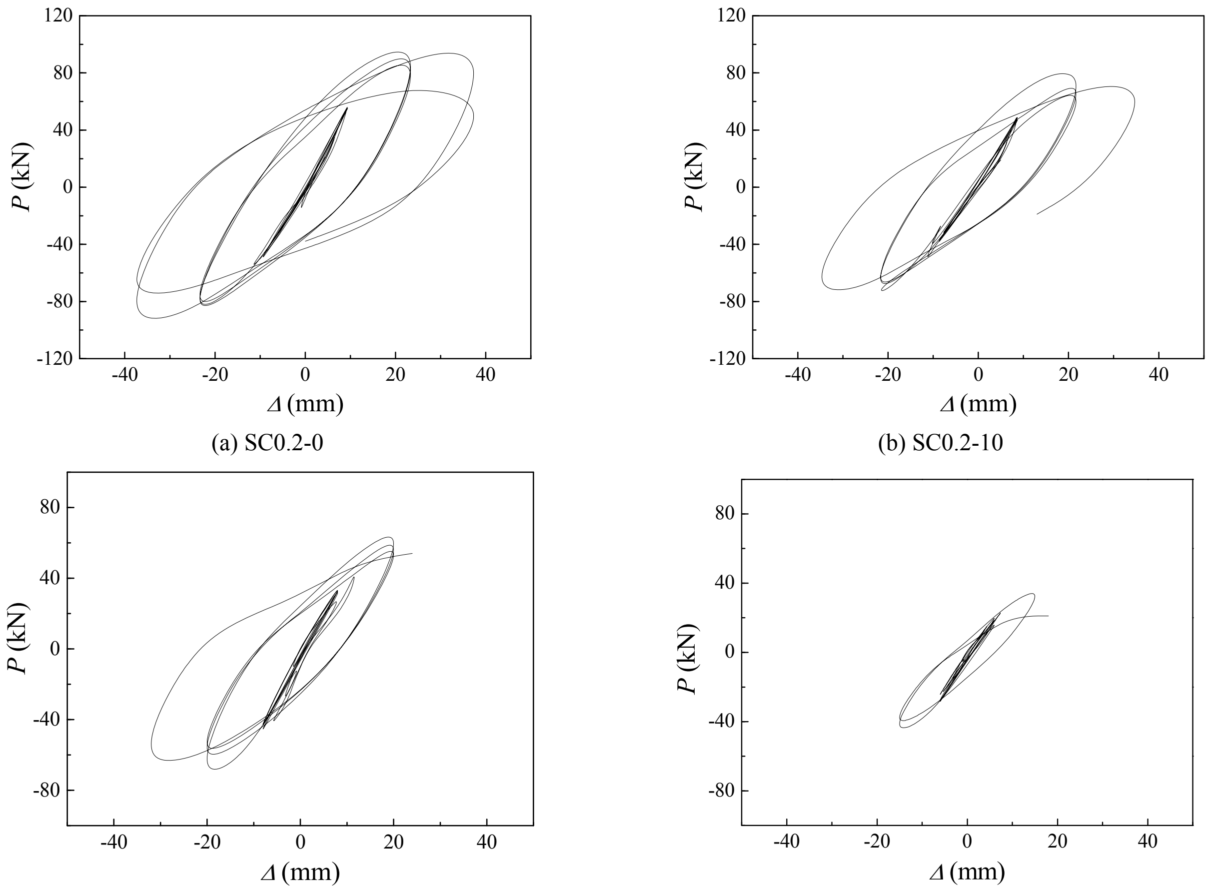

(a) SC0.2-0 (b) SC0.2-10

(c) SC0.2-20 (d) SC0.2-30

Fig. 8 Cyclic load-displacement curves of the specimens

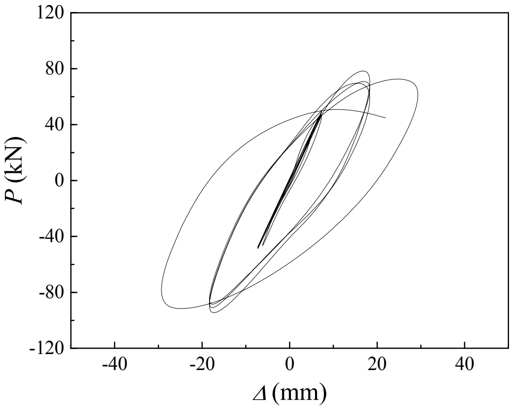

(e) SC0.4-0

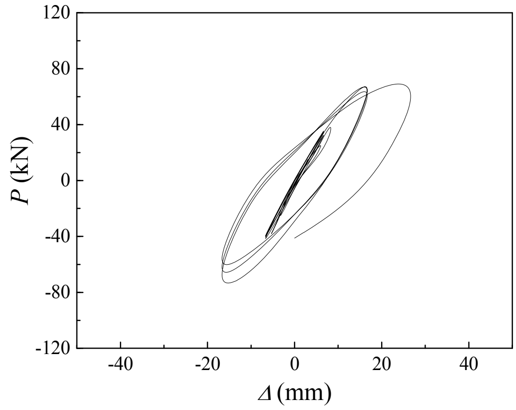

(f) SC0.4-10

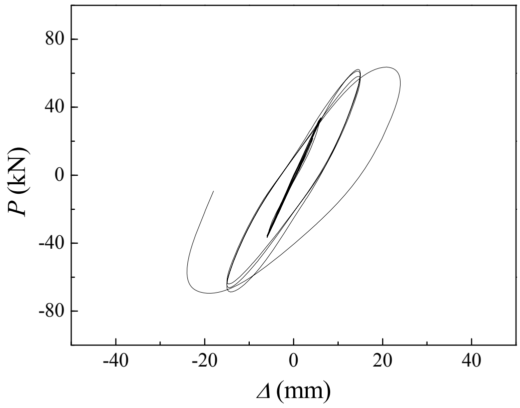

(g) SC0.4-20

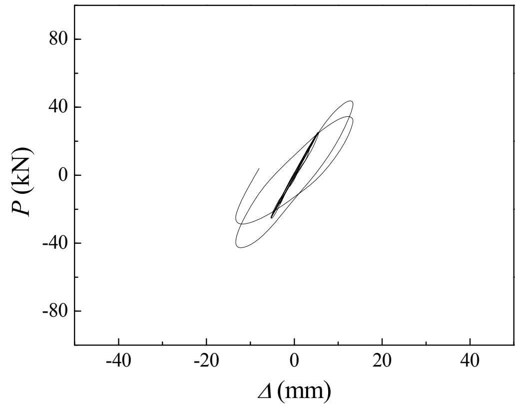

(h) SC0.4-30

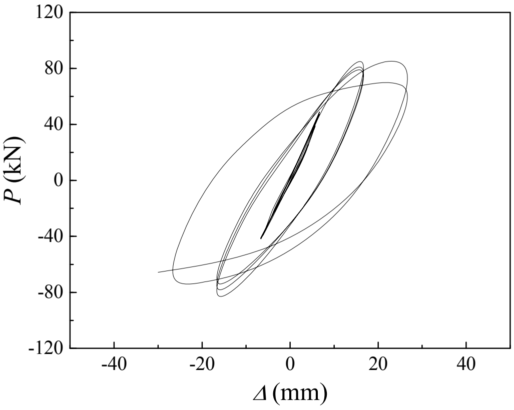

(i) SC0.5-0

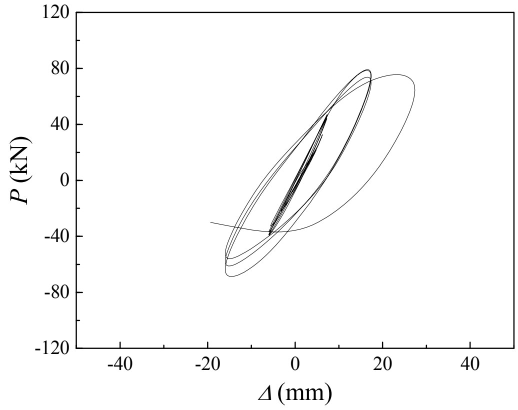

(j) SC0.5-10

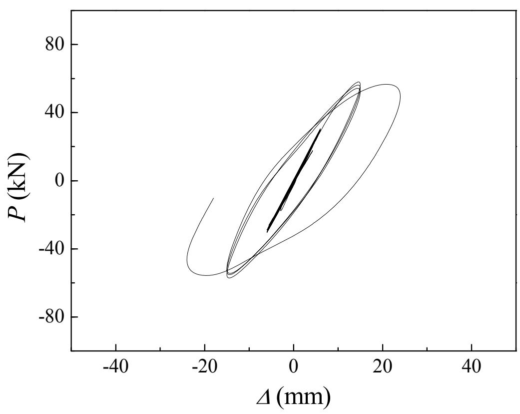

(k) SC0.5-20

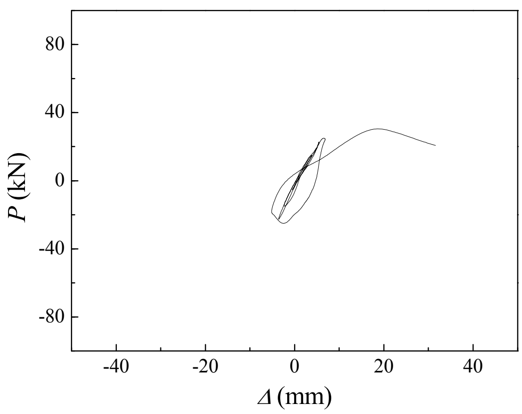

(l) SC0.5-30

Fig. 8 Continumed

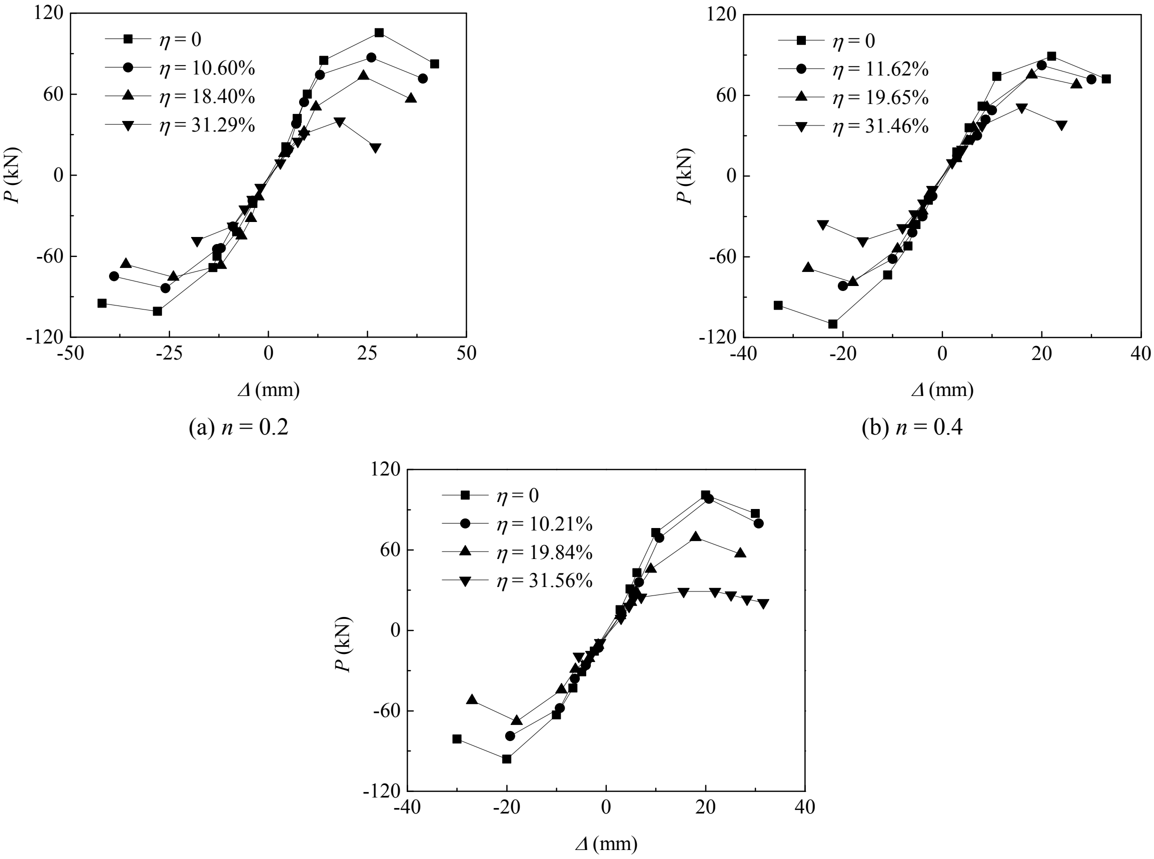

(a) $n = 0.2$ (b) $n = 0.4$

(c) $n = 0.5$

Fig. 9 Effect of corrosion rate (η) on the load-displacement envelop curves of the specimens

ultimate lateral strength (P_u) and ultimate displacement (Δ_u) of the CFST columns with an axial force ratio of 0.4 are reduced by 48.3% and 56.5% as the corrosion rate increases from 0 to 31.46%, respectively, where P_u refers to the peak lateral load, and Δ_u is defined as the point where the load resistance drops to 85% of its peak value. This definition of ultimate displacement has also been typically employed in other studies (Priestley and Park 1987, Wu *et al*. 2006). The reductions of P_u and Δ_u are attributed to the losses of the wall thickness and yield strength of steel tubes caused by corrosion. Table 1 shows the detailed test results for all specimens. The ultimate displacement of specimen SC0.5-30 was unfortunately not obtained from the test owing to the brittle tensile fracture of the steel tube, and subsequently the sudden drop in the lateral load resistance.

Fig. 10 shows the effects of the axial force ratio on the ultimate strength and ultimate displacement of the specimens. It is found that the axial force ratio has an adverse influence on both the ultimate lateral strength and ultimate displacement of the specimens. The decreasing

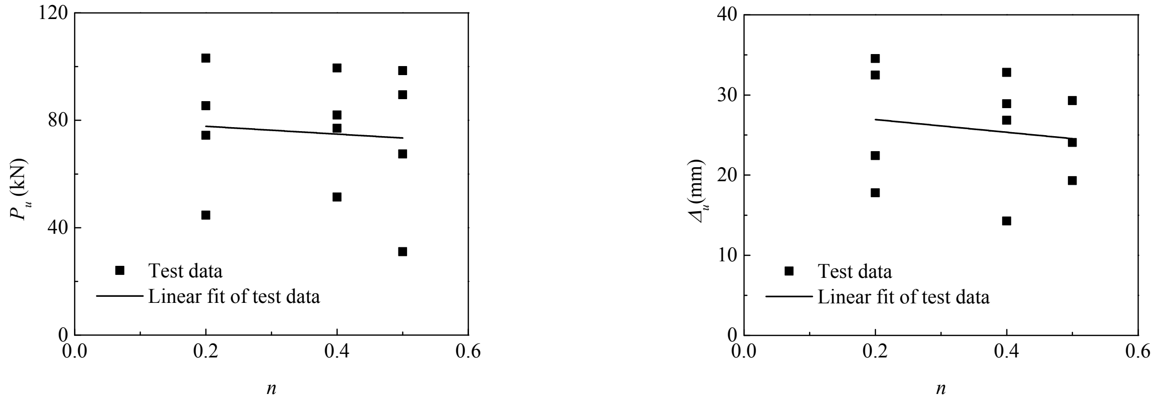

(a) Effect of n on ultimate strength P_u (b) Effect of n on ultimate displacement Δ_u

Fig. 10 Effect of axial force ratio (n) on the global response of the columns

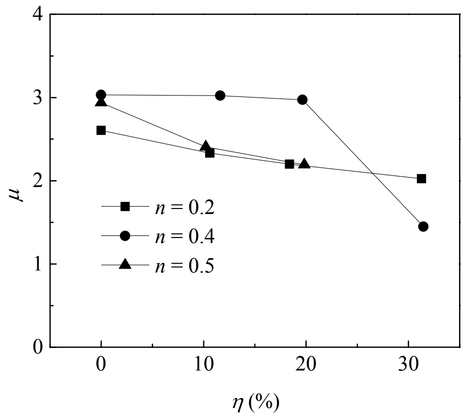

Fig. 11 Effect of corrosion rate (η) on the ductility (μ) of the specimens

trend of the ultimate displacement is more pronounced than ultimate lateral strength as axial force ratio increases. The deformation capacity of the reinforced concrete columns also generally decreases as the axial force ratio increases. For CFST columns with a higher axial force ratio, the compression side tends to buckle more quickly owing to the larger compression load. As a result, the lateral load tends to drop more rapidly under a relatively smaller lateral deformation.

3.4 Ductility and energy dissipation capacity

The ductility coefficient (μ) herein is defined as the ratio of the ultimate displacement to the yield displacement of CFST columns (Δ_u/Δ_y). The effect of the axial force ratio on the ductility coefficient μ for each specimen is shown in Fig. 11. The ductility of the CFST columns at each axial force level decreases evidently as the corrosion rate increases. Both the yield displacement and the ultimate displacement of the columns decrease with an increase in η owing to the reduction of the wall thickness and confinement factor ξ caused by corrosion, as shown in Table 1. However, the deterioration of the ultimate displacement is more pronounced than that of the yield displacement, resulting in a lower ratio of Δ_u/Δ_y and thus a smaller μ for a larger η. The steel tube buckling and the corresponding ultimate state occur earlier for a smaller ξ owing to the weaker composite effect between the core concrete and steel tube.

The cumulative energy dissipation for each specimen is shown in Fig. 12. In the present work, the cumulative dissipated energy at each displacement level is calculated by the sum of the areas of hysteresis loops up to the specific displacement step. Because all specimens deform in a ductile manner, the cumulative dissipated energy shows a steady increase until failure for each specimen. It is found from Fig. 12 that the cumulative dissipated energy exhibits

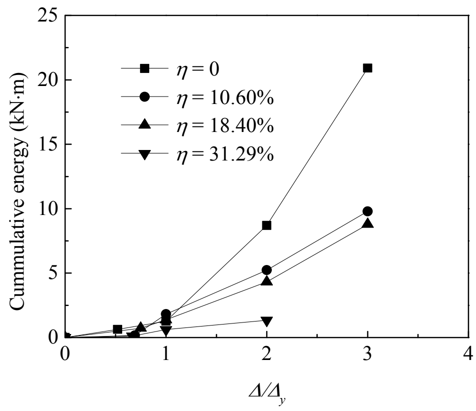

(a) n = 0.2

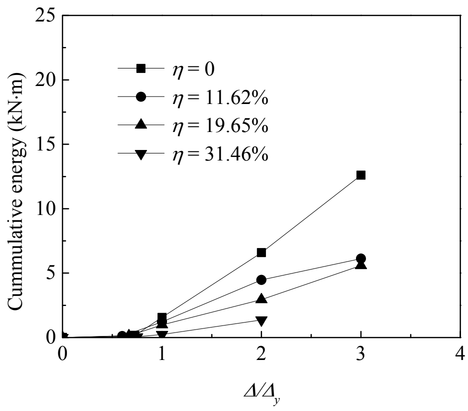

(b) n = 0.4

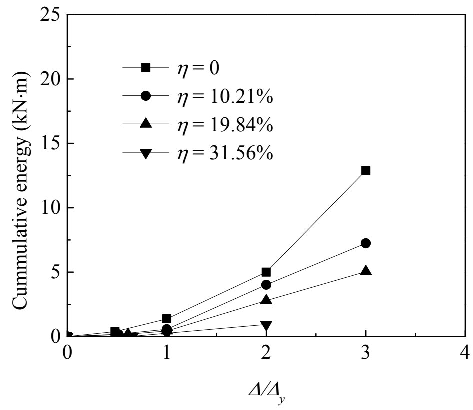

(c) n = 0.5

Fig. 12 Effect of corrosion rate (η) on the cumulative dissipated energy of the specimens an evident decrease with an increase in the corrosion rate. The cumulative dissipated energy levels are close to each other before the yield point at each axial force level. After the yield point, however, the gap in the cumulative energy between the corroded specimens and uncorroded specimens becomes increasingly larger as the displacement level (Δ_u/Δ_y) increases. This indicates that the composite action between the core concrete and steel tube has significant influence on the energy dissipation capacity. As mentioned above, the confinement factor ξ decreases substantially owing to the reduction caused by a corrosion of the wall thickness and yield strength for the outer steel tubes. As ξ decreases, the compressive strength is reduced, and the steel tube buckling occurs earlier, which weakens the energy dissipation capacity of CFST columns at larger displacement levels.

4. Ultimate strength analysis

To evaluate the feasibility of using conventional design methods to calculate the strength of CFST under loading and acid rain attack, design codes GB50936 (2014), DB36/J001 (2007), AIJ (1997), and EC4 (2004) are used to predict the ultimate strength of the tested CFST specimens. The ultimate lateral strength (P_{uc}) of a specimen predicted at each specified axial load level is calculated through the axial force (N) versus moment (M) interaction equations provided in these design codes. Table 3 shows the calculation results, where only the wall thickness loss caused by acid rain corrosion was considered, whereas Table 4 shows the calculation results where the losses in both the wall thickness and yield strength of a steel tube caused by acid rain corrosion were taken into account. For the corroded specimens, the cross-sectional area of a steel tube after corrosion was calculated as

$$A_s = 4(B - 2\Delta t_s)(t_{s0} - \Delta t_s) \tag{4}$$

where Δt_s is the loss in steel tube thickness owing to corrosion. The yield strength of steel after corrosion, based on Yuan *et al*. (2018), was calculated as

$$f_y = (1 - 1.007\eta) f_{y0} \tag{5}$$

where f_y and f_{y0} are the yield strength of corroded and uncorroded steel, respectively.

The comparison between the predicted ultimate lateral strengths using the four codes and the measured ultimate lateral strength (P_{ue}) is shown in Tables 3 and 4. The mean value of the ratio P_{uc}/P_{ue} and the corresponding standard deviation are also presented. It can be seen from Table 3 that, when only the loss in wall thickness of a steel tube caused by corrosion is considered, the AIJ (1997) and EC4 (2004) codes are conservative in predicting the ultimate strength of CFST columns, whereas the GB50936 (2014) and DB36/J001 (2007) codes overestimate the ultimate strength of the CFST columns. GB50936 (2014) provides 15.7% higher strength than the measured ultimate strength, with a standard deviation of 0.334. DB36/J001 (2007) provides 7.5% higher strength than the measured ultimate strength, with a standard deviation of 0.344. However, when the losses in both wall thickness and yield strength of a steel tube caused by corrosion are considered, the ultimate strengths predicted by the GB50936 (2014) and DB36/J001 (2007) codes are very close to the measured results, as shown in Table 4. GB50936 (2014) provides 2.8% higher strength than the measured ultimate strength, with a standard deviation of 0.261. In contrast, DB36/J001 (2007) provides 0.2% lower strength than the measured ultimate strength, with a standard deviation of 0.305. These results further verify the viewpoint that not only the loss in wall

Table 3 Comparisons of ultimate lateral strength (considering only thickness loss caused by corrosion)

Specimen ID	Measured lateral strength P_{ue} (kN)	Predicted lateral strength P_{uc} (kN)				P_{uc}/P_{ue}			
		GB50936 (2014)	DB36/J001 (2007)	AIJ (1997)	EC4 (2004)	GB50936 (2014)	DB36/J001 (2007)	AIJ (1997)	EC4 (2004)
SC0.2-0	103.15	111.33	108.18	97.62	91.98	1.08	1.05	0.95	0.89
SC0.2-10	85.41	101.36	98.42	86.31	81.32	1.19	1.15	1.01	0.95
SC0.2-20	74.40	94.08	91.81	78.51	73.98	1.26	1.23	1.06	0.99
SC0.2-30	44.63	81.66	81.59	65.97	62.16	1.83	1.83	1.48	1.39
SC0.4-0	99.50	91.74	81.14	49.54	68.98	0.92	0.82	0.50	0.69
SC0.4-10	82.00	82.89	73.27	43.37	60.40	1.01	0.89	0.53	0.74
SC0.4-20	77.08	76.44	68.00	39.15	54.52	0.99	0.88	0.51	0.71
SC0.4-30	51.40	64.07	61.04	33.35	46.43	1.30	1.19	0.65	0.90
SC0.5-0	98-.50	76.45	67.61	32.61	57.49	0.78	0.69	0.33	0.58
SC0.5-10	89.50	69.96	61.81	29.02	51.16	0.78	0.69	0.32	0.57
SC0.5-20	67.50	63.70	56.67	25.77	45.43	0.94	0.84	0.38	0.67
SC0.5-30	31.60	55.89	50.86	21.95	38.70	1.80	1.64	0.71	1.25
Mean						1.157	1.075	0.703	0.861
Standard derivation						0.334	0.344	0.340	0.246

Table 4 Comparisons of ultimate lateral strength (considering reduction of both thickness and yield strength)

Specimen ID	Measured lateral strength P_{ue} (kN)	Predicted lateral strength P_{uc} (kN)				P_{uc}/P_{ue}			
		GB50936 (2014)	DB36/J001 (2007)	AIJ (1997)	EC4 (2004)	GB50936 (2014)	DB36/J001 (2007)	AIJ (1997)	EC4 (2004)
SC0.2-0	103.15	111.33	108.18	97.62	91.98	1.08	1.05	0.95	0.89
SC0.2-10	85.41	91.73	91.31	77.26	72.80	1.07	1.07	0.90	0.85
SC0.2-20	74.40	78.62	81.47	64.53	60.80	1.06	1.09	0.87	0.82
SC0.2-30	44.63	69.26	74.54	55.32	52.13	1.55	1.67	1.24	1.17
SC0.4-0	99.50	91.74	81.14	49.54	68.98	0.92	0.82	0.50	0.69
SC0.4-10	82.00	75.01	68.02	38.83	54.07	0.91	0.83	0.47	0.66
SC0.4-20	77.08	63.89	60.47	32.19	44.83	0.83	0.78	0.42	0.58
SC0.4-30	51.40	56.89	55.80	27.97	38.95	1.11	1.08	0.54	0.76
SC0.5-0	98.50	76.45	67.61	32.61	57.49	0.78	0.69	0.33	0.58
SC0.5-10	89.50	63.32	57.33	25.97	45.79	0.71	0.64	0.29	0.51
SC0.5-20	67.50	53.24	50.39	21.19	37.36	0.79	0.75	0.31	0.55
SC0.5-30	31.60	47.41	46.50	18.41	32.46	1.53	1.50	0.59	1.04
Mean						1.028	0.998	0.618	0.758
Standard derivation						0.261	0.305	0.290	0.196

thickness but also the reduction in yield strength of an outer steel tube caused by corrosion should be taken into account when predicting the ultimate strength of corroded CFST members as a design safety improvement.

It is also noted that even if the strength deterioration is considered, the strength prediction error for columns with corrosion rate of 30% can be up to 50% by using DB36/J001 (2007) and EC4 (2004). The failure process becomes more brittle for a higher corrosion rate owing to the weaker composite effect between the core concrete and steel tube. As the corrosion rate reaches as high as 30%, the strength failure of the CFST column is caused by not only material failure factor but also somewhat stability failure factor.

5. Conclusions

This paper described the testing of the mechanical behaviours of CFST columns under an acid rain attack and a cyclic load. The tensile properties of steel coupons were first studied in detail. A reversed cyclic load test was subsequently carried out for both corroded and uncorroded CFST specimens. The effects of corrosion rate η and the axial force ratio were taken into consideration. The following conclusions can be drawn from this study:

- Acid rain corrosion has not only a significant influence on the reduction in wall thickness of a steel tube, but also an adverse effect on the mechanical properties of the steel itself, such as the yield strength f_y, ultimate strength f_u, elastic modulus E_s, and ultimate elongation ε_u. As a result, the loss of strength and deformation capacities of the outer steel tubes caused by corrosion should also be taken into consideration in the prediction of the load carrying capacity of corroded CFST members.
- Corrosion does not change the failure modes of CFST specimens. However, uncorroded CFST columns show a higher load carrying capacity, better ductility, and higher energy dissipation capacity compared with corroded columns. A higher corrosion rate leads to poorer resulting seismic performance of the CFST specimens.
- The axial force ratio has an adverse influence on both the ultimate lateral strength and ultimate displacement of the specimens. The decreasing trend of the ultimate displacement is more pronounced than ultimate lateral strength as axial force ratio increases.
- The ultimate strength measured was compared with the predicted results using the GB50936 (2014), DB36/J001 (2007), AIJ (1997) and EC4 (2004) codes. It was found that, when the losses of both the wall thickness and yield strength of the outer steel tube caused by corrosion are taken into account, the AIJ (1997) and EC4 (2004) codes provide conservative predictions around 25–40% lower than the measured results, whereas the GB50936 (2014) and DB36/J001 (2007) codes provide a very close prediction to the measured results in terms of the ultimate strength.

It should be noted that this study was only focused on the effect of uniform corrosion on the seismic behaviours of a CFST. Localized or pit corrosion, which could occur in a real corrosive environment, was not considered in the current study. This topic will be discussed in future studies.

Acknowledgments

The research described in this paper was financially supported by the National Natural Science Foundation of China (Grant Nos. 51378206 and 51608199).

References

AIJ (1997), Recommendations for Design and Construction of Concrete Filled Steel Tubular Structures; Architectural Institute of Japan, Tokyo, Japan.

Almusallam, A.A. (2001), "Effect of degree of corrosion on the properties of reinforcing steel bars", *Constr. Build. Mater.*, **15**(8), 361-368.

Aslani, F., Uy, B., Tao, Z. and Mashiri, F. (2015), "Predicting the axial load capacity of high-strength concrete filled steel tubular columns", *Steel Compos. Struct., Int. J.*, **19**(4), 967-993.

Aslani, F., Uy, B., Hur, J. and Carino, P. (2017), "Behaviour and design of hollow and concrete-filled spiral welded steel tube columns subjected to axial compression", *J. Constr. Steel Res.*, **128**, 261-288.

Boyd, P.F., Cofer, W.F. and Mclean, D.I. (1995), "Seismic performance of steel-encased concrete columns under flexural loading", *ACI Struct. J.*, **92**(3), 355-364.

Chen, M.C., Wang, K. and Xie, L. (2013), "Deterioration mechanism of cementitious materials under acid rain attack", *Eng. Fail. Anal.*, **27**(1), 272-285.

DB36/J001 (2007), Technical specification for concrete filled steel tubular structures; The Construction Department of Jiangxi Province, Jiangxi, China. [In Chinese]

Elremaily, A. and Azizinamini, A. (2002), "Behavior and Strength of Circular Concrete-Filled Tube Columns", *J. Constr. Steel Res.*, **58**(12), 1567-1591.

Eurocode 4 (2004), Design of composite steel and concrete structures. Part 1-1: general rules and rules for building; EN 1994-1-1:2004. European Committee for Standardization, Brussels, Belgium.

Evirgen, B., Tuncan, A. and Taskin, K. (2014), "Structural behavior of concrete filled steel tubular sections (CFT/CFSt) under axial compression", *Thin Wall. Struct.*, **80**, 46-56.

Fernandez, I., Bairán, J.M. and Marí, A.R. (2015), "Corrosion effects on the mechanical properties of reinforcing steel bars. Fatigue and σ–ε behavior", *Constr. Build. Mater.*, **101**, 772-783.

Fernandez, I., Bairán, J.M. and Marí, A.R. (2016), "Mechanical model to evaluate steel reinforcement corrosion effects on σ–ε and fatigue curves. Experimental calibration and validation", *Eng. Struct.*, **118**, 320-333.

GB50936 (2014), Technical code for concrete filled steel tubular structures; Ministry of Construction of the People's Republic of China. [In Chinese]

Ghazijahani, T.G., Jiao, H. and Holloway, D. (2017), "Concrete-filled circular steel tubes with a timber infill under axial compression", *J. Struct. Eng.*, **143**(7), 04017037.

Hajjar, J.F., Molodan, A. and Schiler, P.H. (1998), "A distributed plasticity model for cyclic analysis of concrete-filled steel tube beam-columns and composite frames", *Eng. Struct.*, **20**(4-6), 398-412.

Han, L.H., Zhao, X.L. and Tao, Z. (2001), "Tests and mechanics model for concrete-filled SHS stub columns, columns and beam-columns", *Steel Compos. Struct., Int. J.*, **1**(1), 51-74.

Han, L.H., Hou, C. and Wang, Q.L. (2012), "Square concrete filled steel tubular (CFST) members under loading and chloride corrosion: experiments", *J. Constr. Steel Res.*, **71**(1), 11-25.

Han, L.H., Hou, C. and Wang, Q.L. (2014), "Behavior of circular CFST stub columns under sustained load and chloride corrosion", *J. Constr. Steel Res.*, **103**, 23-36.

Hill, J., Byars, E.A., Sharp, J.H., Lynsdale, C.J., Cripps, J.C. and Zhou, Q. (2003), "An experimental study of combined acid and sulfate attack of concrete", *Cem. Concr. Compos.*, **28**(8), 997-1003.

Hou, C.C., Han, L.H., Wang, Q.L. and Hou, C. (2016), "Flexural behavior of circular concrete filled steel tubes (CFST) under sustained load and chloride corrosion", *Thin Wall. Struct.*, **107**, 182-196.

Karagah, H., Shi, C., Dawood, M. and Belarbi, A. (2015), "Experimental investigation of short steel columns with ocalized corrosion", *Thin Wall. Struct.*, **87**, 191-199.

Kharoob, O.F., Ghazy, M.F. and Yossef, N.M. (2017). "Behavior of beam-high performance fiber reinforced CFST column joints", *Thin Wall. Struct.*, **113**, 217-227.

Lahlou, K., Lachemi, M. and Aitcin, P.C. (1999), "Confined high-strength concrete under dynamic compressive loading", *J. Struct. Eng.*, **125**(10), 1100-1108.

Larssen, T., Seip, H.M., Semb, A., Mulder, J., Muniz, I.P., Vogt, R.D., Lydersen, E., Angell, V., Dagang, T. and Eilertsen, O. (1999), "Acid deposition and its effects in China: an overview", *Environ. Sci. Policy*, **2**(1), 9-24.

Melchers, R.E. (2006), "Recent progress in the modeling of corrosion of structural steel immersed in seawaters", *J. Infrastruct. Syst.*, **12**(3), 154-162.

Morishita, Y. and Tomii, M. (1982), "Experimental studies on bond strength between square steel tube and encased concrete core under cyclic shearing force and constant axial force", *T. Jpn. Conc.r Inst.*, **4**, 363-370.

Nakanishi, K., Kitada, T. and Nakai, H. (1999), "Experimental study on ultimate strength and ductility of concrete filled steel columns under strong earthquake", *J. Constr. Steel Res.*, **51**(3), 297-319.

Patel, V.I., Uy, B., Prajwal, K.A. and Aslani, F. (2016), "Confined concrete model of circular, elliptical and octagonal CFST short columns", *Steel Compos. Struct., Int. J.*, **22**(3), 497-520.

Priestley, M.J.N. and Park, R. (1987), "Strength and ductility of concrete bridge columns under seismic loading", *ACI Struct. J.*, **84**(1), 61-76.

Rezaifar, O. and Younesi, A. (2017). "Experimental study discussion of the seismic behavior on new types of internal/external stiffeners in rigid beam-to-CFST/HSS column connections", *Construct. Build. Mater.*, **136**, 574-589.

Saad-Eldeen, S., Garbatov, Y. and Soares, C.G. (2013), "Effect of corrosion severity on the ultimate strength of a steel box girder", *Eng. Struct.*, **49**(2), 560-571.

Sakino, K. and Tomii, M. (1981), "Hysteretic behavior of concrete filled square steel tubular beam-columns failed in flexure", *T. Jpn. Concr. Inst.*, **3**(6), 439-446.

Sultana, S., Wang, Y., Sobey, A.J., Wharton, J.A. and Shenoi, R.A. (2015), "Influence of corrosion on the ultimate compressive strength of steel plates and stiffened panels", *Thin Wall. Struct.*, **96**, 95-104.

Vu, N.A., Castel, A. and François, R. (2009), "Effect of stress corrosion cracking on stress–strain response of steel wires used in prestressed concrete beams", *Corros. Sci.*, **51**(6), 1453-1459.

Wu, Y.F., Liu, T. and Oehlers, D.J. (2006), "Fundamental principles that govern retrofitting of reinforced concrete columns by steel and FRP jacketing", *Adv. Struct. Eng.*, **9**(4), 507-533.

Yuan, F., Chen, M., Huang, H., Xie, L. and Wang, C. (2018), "Circular concrete filled steel tubular (CFST) columns under cyclic load and acid rain attack: test simulation", *Thin Wall. Struct.*, **122**, 90-101.

Nomenclature

The following symbols are used in this paper:

A_c = cross-sectional area of core concrete;

A_{s0} = initial cross-sectional area of steel tube;

A_s = cross-sectional area of steel tube after corrosion;

B = width of tube section;

E_s = elastic modulus of corroded steel;

f_{ck} = characteristic compressive strength of concrete;

f_{cu} = compressive strength of cube concrete;

f_y = yield strength of corroded steel;

f_{y0} = yield strength of uncorroded steel;

f_u = ultimate strength of corroded steel;

n = axial force ratio;

L = column length;

N_0 = axial force applied on the columns;

N_u = axial compressive capacity of the columns;

P = lateral load of column;

P_u = ultimate lateral strength;

P_{uc} = predicted ultimate lateral strength;

P_{ue} = measured ultimate lateral strength;

P_y = yield load;

t_s = wall thickness of steel tube after corrosion;

t_{s0} = initial wall thickness of steel tube;

η = corrosion rate;

ξ = confinement factor;

μ = ductility coefficient;

ε_u = ultimate elongation of corroded steel;

Δ = lateral displacement of column;

Δt_s = wall thickness loss of steel tube owing to corrosion;

Δ_u = displacement when the lateral load falls to 85% of the ultimate strength (P_u);

Δ_y = yield displacement.

BU